1. **Manuscript Title:** V3 Interneurons are Active and Recruit Spinal Motor Neurons During *In Vivo* Fictive Swimming in Larval Zebrafish
2. **Abbreviated Title:** V3 Interneurons Recruit Spinal Motor Neurons
3. **List of Authors:**

   - Timothy D. Wiggin[†], University of Minnesota, Department of Neuroscience, Minneapolis, MN 55455
   - Jacob E. Montgomery[†], University of Minnesota, Department of Neuroscience, Minneapolis, MN 55455
   - Amanda J. Brunick, Bucknell University, Department of Neuroscience, Lewisburg, PA 17837
   - Jack H. Peck, University of Minnesota, Department of Neuroscience, Minneapolis, MN 55455
   - Mark A. Masino, University of Minnesota, Department of Neuroscience, Minneapolis, MN 55455

   [†] Equal contribution and First authorship.

4. **Author Contributions:** TDW, JEM and MAM Designed the Research; TDW, JEM, AJB, JHP and MAM Performed the Research; TDW and MAM Wrote the Paper
5. **Correspondence should be addressed to** Mark A. Masino, masino@umn.edu
6. **Number of Figures:** 6
7. **Number of Tables:** 1
8. **Number of Multimedia:** 0
9. **Number of words for Abstract:** 213
10. **Number of words for Significance Statement:** 120
11. **Number of words for Introduction:** 570
12. **Number of words for Discussion:** 1,292
13. **Acknowledgements:** The authors appreciate the helpful suggestions and feedback from Drs. Ronald Calabrese and Ronald Harris-Warrick. We also thank Kayce Vanpelt for technical support and Marc Tye and the staff of the University of Minnesota Zebrafish Core Facility for animal care. Finally, we thank Drs. Koichi Kawakami and Misha Ahrens for kindly providing *Tg(UAS:GCaMP6s)*$^{nk13a}$ fish. Current affiliation for TDW is Vizgen, Cambridge, MA 02138 and AJB is Florida State University, Department of Psychology, Tallahassee, FL 32306
14. **Conflict of Interest:**
    **(A) No.**
    Authors report no conflict of interest.
15. **Funding Sources:** This work was supported by National Institutes of Health R01 NS065054 (MAM), R01 NS094176 (MAM), F31 NS083110 (TDW), R25 NS083059 (to Dr. Robert Meisel), Regenerative Medicine Minnesota (JEM), and the Grant-in-Aid of Research, Artistry, and Scholarship (MAM).

**ABSTRACT**

Survival for vertebrate animals is dependent on the ability to successfully find food, locate a mate, and avoid predation. Each of these behaviors requires motor control, which is set by a combination of kinematic properties. For example, the frequency and amplitude of motor output combine in a multiplicative manner to determine features of locomotion such as distance traveled, speed, force (thrust), and vigor. Although there is a good understanding of how different populations of excitatory spinal interneurons establish locomotor frequency, there is a less thorough mechanistic understanding for how locomotor amplitude is established. Recent evidence indicates that locomotor amplitude is regulated in part by a subset of functionally and morphologically distinct V2a excitatory spinal interneurons (type II, non-bursting) in larval and adult zebrafish. Here we provide direct evidence, for the first time, that most V3 interneurons (V3-INs), which are a developmentally and genetically defined population of ventromedial glutamatergic spinal neurons, are active during fictive swimming. We also show that elimination of the spinal V3-IN population reduces the proportion of active MNs during fictive swimming but does not alter the range of locomotor frequencies produced. These data are consistent with V3-INs providing excitatory drive to spinal motor neurons and contributing to the production of locomotor amplitude, but not frequency, during swimming in larval zebrafish.

## SIGNIFICANCE STATEMENT

Currently, there is a limited understanding about the cellular and spinal network properties that produce locomotor amplitude, defined as limb displacement in limbed animals or tail-bend in non-limbed animals during locomotion. Here we show, directly for the first time in a vertebrate, that V3 interneurons (V3-INs) in zebrafish larvae are active during *in vivo* fictive locomotion, and that targeted ablation of the spinal V3-IN population reduces the proportion of active motoneurons during fictive swimming. Importantly, ablation of V3-INs does not affect locomotor frequency (speed), which clarifies their role in motor control rather than rhythm generation. Thus, we propose that the V3-IN population is a source of excitation in the vertebrate locomotor neural circuitry that regulates locomotor amplitude independently of speed.

## INTRODUCTION

Efficient locomotion is set by a combination of kinematic properties, including the frequency and amplitude of rhythmic motor output. These properties combine to determine various locomotor features, such as distance traveled, speed, and vigor (Webb, 1975; Jayne and Lauder, 1995; Donley and Dickson, 2000; Tytell, 2004). Locomotor frequency (e.g. limb or tail-beat rhythmic activity) is a well-studied kinematic variable, which has been shown to increase linearly with speed (Bainbridge, 1958; Hunter and Zweifel, 1971; Webb et al., 1984; Müller and van Leeuwen, 2004). Less well studied is locomotor amplitude, which is measured by limb displacement in limbed animals during locomotor events (walking, trotting, galloping, hopping (Heglund et al., 1974)) or by tail-bend in non-limbed animals during anguilliform swimming (Wardle et al., 1995; Videler et al., 1999). Although there is a fundamental understanding of how identified subsets of excitatory spinal interneurons help to establish the frequency of motor output (Crone et al., 2009; Zhong et al., 2011; Ausborn et al., 2012; Eklöf-Ljunggren et al., 2012; Kimura et al., 2013; Ampatzis et al., 2014; Ljunggren et al., 2014; Menelaou et al., 2014; Bellardita and Kiehn, 2015), a more complete understanding of the cellular and network properties that regulate locomotor amplitude in vertebrate animals is lacking.

Across vertebrate species from fish to mammals, the neural circuitry that controls locomotion is located in the ventromedial spinal cord (Grillner and Jessell, 2009; Kiehn, 2011). In vertebrates, developmental gene expression specifies at least five cardinal classes of ventral neuronal progenitor cells. These progenitors give rise to motor neurons (MNs) and four classes of ventral interneurons, referred to as V0 to V3 neurons (Ericson et al., 1997; Pierani et al., 1999). Over the past decade, a population of identified

54 excitatory spinal interneurons (V2a) has been shown to control the speed of locomotion
55 in a variety of vertebrates (Zhong et al., 2011; Ausborn et al., 2012; Ampatzis et al.,
56 2014; Gosgnach et al., 2017). More recent studies indicate a role for a subset of V2a
57 interneurons (type II, non-bursting) in regulating locomotor amplitude (Menelaou and
58 McLean, 2019) and/or vigor (Song et al., 2018) in larval and adult zebrafish, respectively.
59 Both studies reveal a hierarchical control of motor neuron recruitment by a diverse V2a
60 interneuron population, which the authors conclude is the basis for regulating locomotor
61 amplitude and/or vigor.

62 To date, a cardinal class of spinal interneurons in the ventral cord that selectively
63 regulates locomotor amplitude independently of locomotor frequency has not been
64 identified. In the mammalian spinal cord, a genetically defined population of pre-motor
65 glutamatergic neurons, called V3 interneurons (V3-INs), contributes to limb
66 coordination, motor burst duration, and muscle spasms, but does not have a clear role in
67 locomotor pattern generation (Chopek et al., 2018; Danner et al., 2019; Lin et al., 2019).
68 We hypothesized V3-INs provide excitatory drive during locomotor activity to regulate
69 locomotor amplitude. The work presented here shows directly, for the first time, that V3-
70 INs in zebrafish larvae are active during *in vivo* fictive locomotion, and that elimination
71 of the V3-IN spinal population reduces the proportion of active MNs during fictive
72 swimming but does not alter the range of locomotor frequencies produced. These data are
73 consistent with V3-INs providing excitatory drive to spinal motor neurons and
74 contributing to the production of locomotor amplitude, but not frequency, during
75 swimming in larval zebrafish. This is conceptually important because it clarifies a role of

76 the V3 cardinal class of spinal interneurons in motor control, rather than rhythm
77 generation.
78
79 **MATERIALS AND METHODS**
80 *Fish Lines and Maintenance*
81 All animal procedures were performed in accordance with the animal care
82 committee's regulations. Wild type (Segrest Farms, Gibsonton, FL) and transgenic adult
83 zebrafish (*Danio rerio*) were maintained in the animal facility. The transgenic lines used
84 in these experiments were: *Tg(nkx2.2a:mEGFP)*$^{vu17}$ (Kirby et al., 2006),
85 *Tg(vglut2a:DsRed)*$^{nns9}$ (Miyasaka et al., 2009), *Tg(vglut2a:Gal4ff)*$^{nns20}$ (Satou et al.,
86 2013), *Tg(UAS:GCaMP6s)*$^{nk13a}$ (Muto et al., 2017), and *parga*$^{mn2Et}$ (Balciunas et al.,
87 2004). Out-crossed transgenic larvae at 4 – 6 days post fertilization (dpf) were used in
88 these experiments. Larval zebrafish were maintained in petri dishes filled with embryo
89 water (60 µg/ml Instant Ocean® salt mix, Cincinnati, OH) and 0.00005% Methylene Blue
90 in a 28.5°C incubator with a 14:10 light:dark cycle (ZT0 = 8:30am).
91
92 *V3-IN Soma Distribution Analysis*
93 Quantification of the distribution of V3-IN cell bodies was performed using Fiji
94 and custom Matlab code (Mathworks, Natick, MA). Confocal microscopy was used to
95 collect overlapping stacks of images documenting the expression of
96 *Tg(vglut2a:DsRed)*$^{nns9}$ and transmitted light morphology. Images were acquired at high
97 magnification (40X / NA 0.8 objective) and a z-axis resolution of 1.3 µm. The fields of
98 view in each stack overlapped with their neighbors by at least 10% of the width to permit

accurate stitching and included the full width of the spinal cord and dorsal root ganglia (DRG) in the field of view. The collection of stacks was stitched into a single 3-D image of the caudal hindbrain and spinal cord (Preibisch et al., 2009). The Fiji Cell Counter tool (Schindelin et al., 2012)was used to identify the coordinates of all V3 neurons in the rostral 2 mm of the larval spinal cord (out of a total length of ~3 mm), the coordinates of the DRG neuron clusters, and the position of the dorsal and ventral edges of the spinal cord. The markers tracing the dorsal and ventral edges of the spinal cord were used to calculate local tangent lines to the dorsal and ventral edges of the spinal cord at the rostrocaudal position of each V3-IN. The equation of a line perpendicular to the ventral tangent and intersecting the V3-IN was calculated, referred to as the "V3 plumb line." The rostrocaudal distance of each V3 neuron was calculated as the distance along the ventral surface of the spinal cord between the spinal cord/hindbrain junction (Segment 2/3 boundary) and the V3 plumb line intersection with the ventral surface. The dorsoventral height of the spinal cord at the location of each V3-IN was calculated as the distance between the intersections of the V3 plumb line with the dorsal surface and the ventral surface, respectively. The distance of the V3-IN from the ventral surface of the spinal cord was also measured along the plumb line. The z-axis position of DRG neurons on each side of the spinal cord were used as boundary points of the lateral edges of the spinal cord, and a linear fit to the DRG neurons on each side of the animal was used to calculate the edges of the spinal cord at each rostrocaudal position in the imaging area. The midline slice and spinal cord width were calculated at the rostrocaudal position of each V3-IN, along with the distance from midline of the V3-IN.

122 *Whole-mount Immunohistochemistry*

123 Five dpf *parga*$^{mn2Et}$ larvae were sacrificed with 0.2% Tricaine-S and fixed
124 overnight in 4% paraformaldehyde at 4°C. Whole-mount larvae were permeabilized with
125 Proteinase K, post-fixed, and blocked with 0.2% BSA, 10% normal donkey serum, 0.5%
126 Triton X-100 in PBS. Goat polyclonal anti-choline acetyltransferase (ChAT; 1:50;
127 AB144P) was added to the blocking solution and incubated overnight at 4°C. Fixed
128 larvae were incubated with Alexa Fluor 633 donkey anti-goat secondary antibody (1:500;
129 A-21082, Thermo Fisher Scientific Inc., Waltham, MA) in secondary blocking solution
130 (0.2% BSA, 1% normal donkey serum, 0.5% Triton X-100 in PBS) for three nights at
131 4°C.

132 Anti-ChAT labeled *parga*$^{mn2Et}$ larvae were embedded laterally in low melting-
133 point agarose. An Olympus Fluoview FV1000 confocal microscope was used to collect
134 images through a 60x objective centered on body segment 15. Confocal stacks contained
135 the entire dorsoventral extent of the spinal cord and spanned approximately three body
136 segments (285 µm). Images were processed in Fiji and labeled cells from a single side of
137 the spinal cord (approximately three hemisegments) were quantified using the Cell
138 Counter plugin. Photoshop CS5 (Adobe Systems, San Jose, CA) was used to adjust
139 brightness and contrast across entire z-projected images.

140

141 *In Vivo Rhod-2 AM Dye Loading of Motor Neurons*

142 For *in vivo* characterization of MNs in *parga*$^{mn2Et}$ larvae, a 0.25% Rhod-2 AM
143 (Life Technologies, Grand Island, NY) stock was made by dissolving 50 µg of dye in 20
144 µL Pluronic F-127:DMSO (1:4; Life Technologies, Grand Island, NY). Next, the skin

145 was removed from the midbody region and a 1:50 dilution of the Rhod-2 AM stock was
146 bath applied to the exposed muscles to permit sequestration of indicator dye by MNs via
147 the peripheral motor axons. Sensory neurons were not strongly loaded by this procedure.
148 Following one-hour incubation, the Rhod-2 AM solution was thoroughly washed-out
149 using zebrafish ringers solution. Confocal images were collected, and cells were
150 quantified as described for whole-mount immunohistochemistry (above).
151
152 *Peripheral Nerve Recordings and Analysis*
153 Zebrafish larvae were anesthetized, the skin was carefully removed from the
154 recording region, and larvae were paralyzed with of 0.1 mM α-bungarotoxin (Tocris,
155 Ellisville, MO) to prevent muscle contractions. The anesthetic was removed to allow the
156 larvae to perform fictive behavior, and a suction electrode (tip diameter: 9-15 μm) was
157 placed over the intermyotomal cleft to record MN axons. Fictive motor bursts were
158 identified and grouped into episodes using custom Matlab code. The program detected
159 the presence or absence of activity at each voltage sample $v(n)$. For each $v(n)$, the
160 algorithm determined a voltage autocorrelation $c_n(k)$ over a small window (3 ms)
161 centered at $v(n)$. These "windowed" autocorrelations were computed as $c_n(k) =$
162 $\sum_{i=-N0}^{i=N_0} v(n-i)v(n-i-k)$ (*Eq. 1*), where 3-ms windowing was implemented in *Eq.*
163 *1* by setting $N_0 = (3\text{ ms}\cdot f_{\text{sam}})/2$, where $f_{\text{sam}}$ is the sampling frequency, and by setting $v(j) =$
164 0 for $j$ outside the interval $[n - N_0, n + N_0]$.
165 A subset of the autocorrelation values (lags) from *Eq. 1* were used to compute a
166 test statistic for each $v(n)$ with the same lags ($\vec{k}_0 = [k_1, k_2, \ldots, k_m]$) used for all voltage
167 samples. Building on *Eq. 1*, for each $v(n)$, a test statistic $c_n$ was computed as $c_n =$

168 $\sum_{k=k1}^{k=k_m} \sum_{i=-N0}^{i=N_0} v(n-i)v(n-i-k)$ (*Eq. 2*), where *Eq. 2* is the sum of the $c_n(k)$ from *Eq.*

169 *1* specified by $\vec{k_0}$. $\vec{k_0}$ was set at $\vec{k_0} = [1, 2]$ because we found that these values

170 effectively separate the distributions of the test statistics $\{c_n\}$ for samples of noise and

171 samples of activity across a broad range of recording quality.

172 Finally, activity was considered present at $v(n)$ only when $c_n$ was greater than a

173 detection threshold *T*. *T* was set as the maximum of a set of $\{c_n\}$ corresponding to the

174 $\{v(n)\}$ in one contiguous second of the voltage recording where activity was confirmed to

175 be absent (typically the first second of the recording), and was set this way for each

176 individual voltage recording to account for differences in baseline noise levels. Fictive

177 locomotor bursts were detected and grouped into episodes, and the burst and episode

178 properties were determined as follows. Episode duration is the time from the onset of the

179 first burst of an episode to the offset of the final burst in the same episode. Burst duration

180 is the time from the onset to the offset of each burst, as defined by $c_n$ and described

181 above. Burst frequency is the inverse of the interburst period (IBP), which is defined for

182 each pair of bursts within episodes as the time from the onset of the first burst to the onset

183 of the second burst. Peak burst frequency is the inverse of burst period, which is defined

184 as the shortest time duration from onset of one burst to onset of the subsequent burst in an

185 episode of fictive swimming. IBPs between episodes are excluded from burst frequency

186 analysis.

187

188 *Calcium Imaging and Analysis*

189 For calcium imaging of V3-INs, *Tg(vglut2a:Gal4ff)*$^{nns20}$*;Tg(UAS:GCaMP6s)*$^{nk13a}$

190 zebrafish larvae were used. For calcium imaging of MNs, Calcium Green-1 AM (Life

191 Technologies, Grand Island, NY) dye was loaded into MNs using the protocol for Rhod-2
192 AM dye loading described above. Larvae were transferred to a fixed-stage Olympus
193 BX51 WI upright microscope with either a 20x / NA 0.5 or a 40x / NA 0.8 water dipping
194 objective lens. A field of view containing *GCaMP6s*-expressing V3-INs in transgenic
195 larvae or Calcium Green-1 AM-loaded MNs in wild type larvae was selected for calcium
196 imaging and a simultaneous peripheral nerve (PN) recording was acquired. Calcium
197 indicator fluorescence was excited with an E-Cite Series 120 Q lamp (Excelitas
198 Technologies, Waltham, MA) and acquired at 20 Hz with a Retiga EXi camera and
199 QCapture Pro 6.0 software (QImaging, Surry, BC). Data were acquired during
200 spontaneous fictive swimming in 10-60 s durations for both V3-IN and MN trials.
201 Multiple trials (typically 4) were acquired for each field of view, with at least five min
202 between trials. Movement artifacts during data acquisition were corrected in Fiji by
203 registering frames from all trials to a common reference image (Preibisch et al., 2009).
204 Optical and electrophysiological data acquisition were synchronized by using the sync
205 output of the stimulator to trigger acquisition of the PN recording.
206 For all calcium imaging experiments, raw fluorescence values were determined
207 by drawing a region of interest around each identified V3-IN or MN soma and using the
208 Plot Z-axis Profile command in Fiji. Fluorescence from a region of interest containing
209 background signal was subtracted from raw soma fluorescence measurements to reduce
210 the effect of photobleaching. Baseline fluorescence ($F_0$) was defined as the mean
211 fluorescence in the first 10 frames of the recording. To calculate $\Delta F/F$, $F_0$ was subtracted
212 from fluorescence for each frame ($F_{(t)}$), then divided by $F_0$; $\Delta F/F = (F_{(t)} - F_{(0)}) / F_{(0)}$. A
213 neuron was considered active if $\Delta F/F$ was 10% or greater.

214

215 *Targeted Laser Ablation of V3-INs*

216 Acute ablation of the V3-INs was performed using a Micropoint pulsed nitrogen
217 pumped dye laser (Andor Technology, Belfast, Northern Ireland). Light ($\lambda$ = 435 nm)
218 was delivered via an Olympus BX51 WI microscope using a 60x / NA 1.0 water dipping
219 objective lens. The laser was focused to apply maximal light intensity to the imaging
220 plane of the microscope, the intensity of the laser was calibrated to produce a 4.5 – 5.0
221 µm hole in a mirror slide (this optimal intensity was determined empirically), and the x-y
222 coordinates of the laser point in the field of view were indicated on a digital display.
223 Three to six dpf *Tg(vglut2a:DsRed)*$^{nns9}$ zebrafish larvae were anesthetized in 0.02%
224 Tricaine in zebrafish ringers solution and embedded laterally in a gel composed of 3%
225 methylcellulose and 0.02% Tricaine in zebrafish ringers saline. A coverslip was placed
226 over the gel and secured at the edges with agarose to stabilize the position of the larvae.

227 Targeted, bilateral laser ablation of DsRed$^{+}$ V3-INs in the ventral spinal cord was
228 performed by positioning the microscope objective such that a neuron was in the x-y
229 position at which the laser was focused. Laser pulses were applied to each V3-IN soma at
230 33 Hz for 10 s. Laser intensity was empirically determined *a priori* such that >95% of the
231 targeted V3-INs were not present 24 h post-ablation. Following the train of laser pulses,
232 the microscope was repositioned to focus on another identified V3-IN, and the protocol
233 was repeated. Larvae were embedded for approximately 50 min in order to perform
234 bilateral ablation of ~140 identified V3-INs between body segment (S) 5 and S20. To
235 confirm that laser ablation of targeted V3-INs was effective and persistent, the lack of
236 DsRed fluorescence in the lesioned spinal cord of *Tg(vglut2a:DsRed)*$^{nns9}$ larvae was

237 confirmed ~24 hours post-ablation. Sham larvae were treated identically to V3 ablation
238 larvae, but the x-y position of the laser was offset by 5 – 20 μm from each V3 cell,
239 producing non-specific damage to neurons other than the V3 population. Rather than kill
240 a specific cell type as a sham control which might have a specific effect, non-specific
241 laser damage was preferred.
242
243 *Statistical Analysis*
244 Statistical analysis of data was performed using two-sample *t*-test, ANOVA test,
245 Holm-Sidak post-hoc test, Kolmogorov-Smirnov test, and least-squares linear regression.
246 Statistical tests were carried out using SigmaPlot 12 and 14 software (SyStat Software,
247 San Jose, CA), Matlab (Mathworks, Natick, MA), or Microsoft Excel (Microsoft, Seattle,
248 WA). An α level of 0.05 was used to determine statistical significance. Data are reported
249 as means and standard deviation (Mean, SD).
250
251 *Software Accesibility*
252 Custom Matlab code for the quantification of the distribution of V3-IN cell bodies
253 and peripheral nerve recording analysis is available upon request.
254
255 **RESULTS**
256 *V3-INs are Individually Identifiable in the Larval Zebrafish Spinal Cord*
257 To characterize the functional roles of V3-INs *in vivo*, it was necessary to reliably
258 target the neurons for recording and perturbation. While there are no published transgenic
259 zebrafish lines that specifically label neurons expressing *sim1a* (the zebrafish V3-IN

260 marker; (Schäfer et al., 2007)), it is possible to infer V3-IN identity from their other
261 characteristics. V3-INs proliferate ventral to the central canal and are glutamatergic
262 (Zhang et al., 2008; Yang et al., 2010). In zebrafish, there is >90% overlap of *vesicular*
263 *glutamate transporter 2* (*vglut2a*) and *sim1a* expression in the ventral spinal cord at the
264 embryonic stage (1.5 dpf) (Yang et al., 2010). However, it is possible that the embryonic
265 ventral glutamatergic neurons migrate or are replaced by a non-V3 population between
266 1.5 dpf and the free-swimming larval stage (>3 dpf).

267 To test the hypothesis that the ventral DsRed+ neurons observed in 4 – 6 dpf
268 *Tg(vglut2a:DsRed)*$^{nns9}$ larvae are V3-INs, we crossed this line to
269 *Tg(nkx2.2a:mEGFP)*$^{vu17}$, which marks p3 progenitor neurons (Briscoe et al., 2000;
270 Schäfer et al., 2007) (Fig. 1A). At 4 – 6 dpf, *nkx2.2a:mEGFP* expression was restricted to
271 the region ventral to the central canal (Fig. 1C). The p3 domain of the zebrafish spinal
272 cord also produces Kolmer-Agduhr (KA) neurons (Yang et al., 2010), and likely other
273 neuronal types, so it was expected that there would be more *nkx2.2a:mEGFP*-expressing
274 neurons than *vglut2a:DsRed*-expressing neurons (Fig. 1B). Approximately 94% of
275 *vglut2a:DsRed*-expressing neurons ventral to the central canal also expressed
276 *nkx2.2a:mEGFP* ($n$ = 6 larvae, 162 neurons), and were therefore confirmed to be V3-INs
277 (Fig. 1D). There was not a significant difference between the dorsoventral position of the
278 *vglut2a:DsRed*-expressing neurons that co-expressed *nkx2.2a:mEGFP* and those that did
279 not (two-sample t-test; $t = 1.6$; $p = 0.10$), so there was not a way to reliably segregate the
280 identified V3-INs, from those that did not express *nkx2.2a:mEGFP*. However, the
281 overwhelming majority of the DsRed$^{+}$ neurons ventral to the central canal were
282 confirmed to be V3-INs. The lack of confirmed transgene overlap in the remaining cells

283 may be due to variegated transgene expression rather than the presence of a non-V3-IN
284 ventral glutamatergic neuronal population. Based on this experiment, we treat the ventral
285 *vglut2a:DsRed*-expressing neurons as the V3-IN population, with the caveat that a small
286 fraction (~6%) may be misidentified.
287
288 *V3-INs are Located in the Ventromedial Spinal Cord and are Distributed Along the*
289 *Rostrocaudal Axis of the Spinal Cord*
290 In mice, the V3-INs migrate following differentiation to form spatially segregated
291 dorsal and ventral populations that have different cellular properties and may be
292 necessary for different behaviors (Borowska et al., 2013). To determine if there are
293 multiple populations of spatially segregated V3-INs in zebrafish larvae, we used confocal
294 microscopy to create 3-D reconstructions of the spinal cords of 4 – 6 dpf
295 *Tg(vglut2a:DsRed)*$^{nns9}$ zebrafish larvae (Fig. 2A-B). The center of each V3-IN soma in
296 the most rostral 2 mm of the spinal cord was tagged, and the distribution of the neurons
297 within the spinal cord was calculated based on the imputed borders of the spinal cord (see
298 *Methods*). Neurons in the far caudal spinal cord were not counted because the dimensions
299 of the spinal cord taper to the extent that it was difficult to determine the location of the
300 central canal and Mauthner axons. All V3-INs ($n$ = 4 larvae; 797 neurons) were located
301 medial of the Mauthner axon (Fig. 2C). V3-IN density was highest in the rostral spinal
302 cord but remained close to 1 cell per 10 µm throughout the cord (Fig. 2D). The V3-IN
303 somas were approximately 5 µm in diameter in the rostrocaudal axis, so a density of ~1
304 cell per 10 µm thoroughly tiled the ventral spinal cord. The majority of V3-INs were
305 located in the most medial and most ventral 25% of the spinal cord (Figs. 2E & F). There

306 was no parasagittal plane through the medial spinal cord that was unoccupied by V3-INs
307 (Fig. 2E), which suggested that the V3-IN population may be considered a midline
308 population. However, the density of V3-INs was not highest at the sagittal midline of the
309 spinal cord, and when cell density was plotted along the population axis, the point of
310 highest density was adjacent to the spinal cord midline (Fig. 2G). Therefore, we propose
311 that distinct left and right populations of V3-INs are present, but that there are not
312 multiple ipsilateral populations of spatially segregated V3-INs in larval zebrafish.
313
314 *The Majority of V3-INs are Active During Spontaneous Fictive Swimming*
315 In mice, there is only indirect evidence supporting temporal correlation between
316 V3-IN activity and locomotion (Borowska et al., 2013). To test the hypothesis that
317 activity in the V3-INs is appropriately timed to provide excitatory drive to MNs during
318 locomotion, we monitored the activity of the V3-INs during spontaneous fictive
319 swimming using a genetically encoded calcium indicator (GCaMP6s; Fig. 3). The
320 activity of V3-INs and fictive locomotor output during spontaneous swimming was
321 measured via simultaneous calcium imaging and peripheral nerve recording using 4 - 6
322 dpf *Tg(vglut2a:Gal4ff)*$^{nns20}$*;Tg(UAS:GCaMP6s)*$^{nk13a}$ larvae (Fig. 3B-C). We found that
323 the majority, 45 of 48 (94%), of V3-INs were active ($\Delta F/F > 10\%$) during spontaneous
324 fictive swimming episodes ($n = 6$ larvae, 15 trials). Therefore, this is the first direct
325 evidence that V3-INs are active during fictive locomotion, which supports the
326 participation of V3-INs in producing locomotor activity.
327

328 *Ablation of V3-INs Does Not Affect Episodic or Burst Properties of Spontaneous Fictive*
329 *Swimming*

330 The previous experiments demonstrated that V3-INs are positioned appropriately
331 and have neurotransmitter phenotype and activity consistent with providing excitatory
332 drive to motor neurons; however, demonstration of the function of the V3 neurons or
333 their necessity for behavior has not been described. To determine whether canonical
334 features of fictive swimming (episode duration, burst (tail-beat) frequency, and burst
335 duration) are modulated by V3-IN activity, we performed laser ablation of a large
336 percentage of the V3-IN population (>95%; ~140 V3-identified somas across body
337 segments 5 to 20; Fig. 4). Three experimental groups were used: 1) The V3 ablation
338 group, in which all V3-INs on both sides of the spinal cord between S5 and S20 were
339 laser ablated ($n$ = 6 larvae; 145 (SD 9.6) neurons per larva). Representative examples of
340 targeted laser ablation efficacy within a restricted region (Fig. 4A-B) and spatial
341 localization (Fig. 4C-D) are shown. 2) The sham ablation group, in which laser pulses
342 were delivered 5 – 20 μm rostral to each identified V3-IN cell body ($n$ = 6 larvae; 130
343 (SD 10.8) sham targets per larva). 3) The unmanipulated control group was not
344 embedded or exposed to laser pulses ($n$ = 6 larvae).

345 The day following laser ablation or sham ablation, fictive swimming was
346 measured using extracellular peripheral nerve recordings. Episode duration, burst
347 frequency, and burst duration were not significantly different between unmanipulated,
348 sham and ablation experimental groups during spontaneous swimming (one-way
349 ANOVAs; all $F < 1.3$; all $p > 0.30$; Table 1). Further, an effect on the coordination of
350 rostrocaudal (ipsilateral) and side-to-side (contralateral) locomotor activity was not

351 observed (data not shown). These results indicate that the population of spinal V3-INs do
352 not play a significant role in establishing episode duration, burst frequency (a proxy for
353 tail-beat frequency), burst duration, or coordination during fictive locomotion in larval
354 zebrafish.
355
356 *Ablation of V3-INs Reduces the Proportion of Active Motor Neurons but Does Not Affect*
357 *Peak Locomotor Frequency During Spontaneous Fictive Swimming*
358 Since the ablation of spinal V3-INs in zebrafish larvae did not affect episode
359 duration, burst frequency, or burst duration (Table 1), we tested the hypothesis that
360 ablation of V3-INs reduces locomotor amplitude by decreasing the number of active MNs
361 during spontaneous fictive swimming. To ablate V3-INs without also photo-damaging or
362 bleaching motor neurons, we used a two-step neuronal targeting strategy. First, V3-INs
363 were identified and ablated using the *Tg(vglut2a:DsRed)* $^{nns9}$ transgenic line. Following
364 recovery from laser ablation, motor neurons were loaded with a cell-permanent calcium
365 indicator, Calcium Green-1, AM. To verify that spinal neurons loaded with AM dye
366 (Calcium Green-1 and/or Rhod-2) were MNs, we first confirmed motor neuronal
367 specificity of GFP expression in the *parga*$^{mn2Et}$ enhancer trap line (Balciunas et al., 2004).
368 *Parga*$^{mn2Et}$ larvae immunolabeled for the cholinergic marker choline acetyltransferase
369 (ChAT) revealed that most GFP-expressing neurons co-labeled with ChAT antibodies (*n*
370 = 5; 91.3% (SD2.1); Fig. 5A-A''). A small percentage of dorsally-positioned ChAT+
371 cells did not colocalize with GFP (4.1% (SD2.8); Fig. 5A-A'', arrowheads); these cells
372 were considered members of a subset of cholinergic spinal interneurons that modulate

373 MN excitability recently identified in zebrafish (Bertuzzi and Ampatzis, 2018). Thus,
374 GFP expression in the *parga*$^{mn2Et}$ enhancer trap line was specific to MNs.
375 Next, to confirm that loading of AM dye was restricted to MNs, the skin was
376 removed from both sides of the body from *parga*$^{mn2Et}$ larvae, in which GFP expression
377 was shown to be limited to MNs (Fig. 5A-A''), and MNs were labeled with Rhod-2 AM
378 dye ($n$ = 4; Fig. 5B-B''). Rhod-2 AM, which was not used for calcium imaging
379 experiments because it did not produce a strong calcium signal, was used as a proxy for
380 Calcium Green-1 AM since the excitation/emission wavelengths of Calcium Green-1 AM
381 overlapped with, and could not be disambiguated from, GFP expressed in *parga*$^{mn2Et}$
382 MNs. The majority of GFP-expressing MNs co-labeled with Rhod-2 AM (84.3%
383 (SD4.3); Fig. 5B-B''). A small percentage of GFP-negative cells contained Rhod-2 AM
384 (5.4% (SD0.5); Fig. 6B-B'', arrowheads). Taken together, these results confirmed that
385 MNs were selectively labeled with AM dye and, therefore, the cell permeable calcium
386 indicator (Calcium Green-1 AM) could be used to monitor *in vivo* calcium activity in
387 spinal MNs.
388 To examine the effects of V3-IN ablation on the production of fictive locomotor
389 vigor, we determined the proportion of spinal MNs that were active during spontaneous
390 fictive swimming episodes. MN activity in *Tg(vglut2a:DsRed)*$^{nns9}$ larvae was measured
391 using *in vivo* calcium imaging by loading MNs with Calcium Green-1 AM, while peak
392 burst frequency during spontaneous fictive locomotor activity was measured using
393 extracellular PN recordings (Fig. 6A-B). We quantified the proportion of active MNs and
394 peak burst frequencies during spontaneous fictive swimming for Control (50 swim
395 episodes, 4 larvae), Sham Ablated (14 swim episodes, 2 larvae), and V3-IN Ablated (59

396 swim episodes, 3 larvae) groups. Importantly, there were no differences in the properties
397 of the fictive swimming produced by these larvae, consistent with our prior experiments
398 (Table 1). Neither the distribution of peak burst frequencies (Kolmogorov-Smirnov test,
399 $D < 0.33$, $p > 0.14$ for all group comparisons; Fig. 6C), nor the mean peak burst
400 frequencies, were different between Control, Sham, and Ablation Groups (Control = 39.0
401 Hz (SD8.5); Sham = 36.4 Hz (SD10.7); Ablated = 39.3 Hz (SD8.9); one-way ANOVA, F
402 = 5.0, $p = 0.08$; Fig. 6D).
403 Assessment of the probability distributions showed that the proportion of active
404 MNs in the Ablated group was significantly reduced compared to both the Control
405 (Kolmogorov-Smirnov test = 0.68, $p < 0.001$) and Sham (Kolmogorov-Smirnov test =
406 0.54, $p = 0.001$) groups (Fig. 6E). The proportion of active MNs was not significantly
407 different between the Control and Sham groups (Kolmogorov-Smirnov test, $D = 0.24$, $p =$
408 0.50; Fig. 6E). Further, V3-IN ablation had a main effect of significantly reducing the
409 proportion of active MNs during spontaneous fictive swimming (Fig. 6F; Control mean =
410 65.2% (SD16.7); Sham mean = 56.6% (SD24.2); Ablated mean = 41.2% (SD15.6); one-
411 way ANOVA, $F = 25.3$; $p < 0.001$). Pairwise multiple comparisons (Holm-Sidak; Fig.
412 6F) revealed significant differences for the proportion of active MNs between both the
413 Control and Ablated groups ($t = 7.02$, $p < 0.001$) and the Sham and Ablated groups ($t =$
414 $2.98$, $p = 0.007$), but significant differences were not found between Control and Sham
415 groups ($t = 1.54$, $p = 0.10$). These results indicate that V3-INs participate in regulating
416 locomotor amplitude by recruitment of spinal MNs but do not regulate burst frequency
417 during spontaneous fictive locomotion.
418

419 **DISCUSSION**

420 The goal of this study was to characterize the potential role of V3-INs in
421 regulating locomotor amplitude in genetically tractable and optically accessible larval
422 zebrafish. Locomotor amplitude is determined by the recruitment of motor units
423 appropriate to the desired movement: small units for fine behaviors and large units for
424 large movements (Zajac and Faden, 1985; Mendell, 2005). This recruitment pattern of
425 small to large motor units, the so-called size principle, is well established in both limbed
426 (mammalian; terrestrial locomotion) and non-limbed (swimming) locomotor systems
427 (Henneman et al., 1965; Gustafsson and Pinter, 1984a, 1984b; Cope and Pinter, 1995;
428 McLean et al., 2007; Gabriel et al., 2011). However, investigations into the pre-motor
429 neural mechanisms that contribute to the regulation of locomotor amplitude have been
430 difficult in mammals for two primary reasons. First, mammalian spinal locomotor circuits
431 are complicated by the requirements to control and coordinate limbs and joints, rather
432 than simply produce a smooth gradient of motion intensity (Grillner, 2003; Grillner and
433 El Manira, 2020). Second, despite recent progress in tool development, *in vivo* functional
434 manipulations of mammalian spinal locomotor circuits using mini-scopes and fiber-optics
435 are both challenging and limited for long-term recordings in freely locomoting animals
436 (Montgomery et al., 2015; Samineni et al., 2017; Canales et al., 2018). Zebrafish larvae
437 provide several advantages over mammalian models for *in vivo* studies: the spinal cords
438 of fish are less complicated than mammals, zebrafish are recognized as a powerful
439 neurogenetic model system, and the translucent nature of zebrafish larvae makes them
440 particularly appropriate for *in vivo* optical methods of investigation. In this study, we
441 found that, unlike the mammalian spinal circuit, V3-INs in the larval zebrafish spinal

442 cord are contained within a single, ventral anatomical domain (Fig. 1-2) and are not
443 necessary to produce the fictive locomotor rhythm (Table 1) (Zhang et al., 2008; Danner
444 et al., 2019). Instead, zebrafish V3-INs are swim-active neurons (Fig. 3) that contribute to
445 the recruitment of motor neurons during fictive locomotion (Fig. 6), and therefore likely
446 participate in the recruitment of motor units during free-moving locomotion.
447
448 *V3-INs are a population of previously uncharacterized ventral vglut2a+ neurons in*
449 *larval zebrafish*
450 Here, we report that almost all ventrally-located neurons labeled by the
451 *Tg(vglut2a:DsRed)*$^{nns9}$ and *Tg(vglut2a:Gal4ff)*$^{nns20}$ transgenic lines are V3-IN cells (Figs.
452 1-4). The V3-INs, a numerous ventromedial population, are distributed across the
453 rostrocaudal axis of the spinal cord (Fig. 2). It is unlikely that the glutamatergic V3-INs
454 include other identified ventrally-located spinal neurons, such as the GABAergic
455 Kolmer-Agduhr cells (Dale et al., 1987; Bernhardt et al., 1992; Montgomery et al., 2016)
456 or the ventral serotonergic neurons (Van Raamsdonk et al., 1996; Brustein et al., 2003;
457 McLean and Fetcho, 2004; Montgomery et al., 2018). For a more full understanding of
458 the structural and functional relationship of the V3-INs, it will be critical to determine if
459 the diversity of cell morphology in the V3-IN cell population is similar to the diversity of
460 V3-INs in the mammalian spinal cord (Borowska et al., 2013; Deska-Gauthier et al.,
461 2020). In mammals, the morphology of V3-IN subtypes is correlated with their circuit
462 function (Borowska et al., 2013). However, we have not found evidence for differential
463 recruitment of V3-INs during fictive swimming at various frequencies (Fig. 3), which
464 would indicate potential functional heterogeneity. It may be that in larval zebrafish V3-

465 INs are a primitive class of excitatory spinal interneurons, as has been previously
466 proposed for *Engrailed1*-expressing inhibitory neurons in zebrafish (Higashijima et al.,
467 2004). However, analysis of cell morphology in zebrafish larvae is complicated by
468 ongoing development in the nervous system and the rostrocaudal developmental gradient
469 (Cole and Ross, 2001). Further experiments are necessary to clarify if different
470 morphologies represent distinct functional sub-types of V3-INs, developmental stages of
471 a single morphological family, or regional specializations of the V3-INs.
472
473 *Zebrafish V3-INs are active during fictive locomotion*
474 Results indicating that V3-IN activity is directly correlated to fictive locomotor
475 activity in vertebrate preparations has not been convincingly presented. In mice, there is
476 indirect evidence indicating temporal correlation between V3-IN activity and locomotion
477 (Borowska et al., 2013). Through simultaneous optical and electrophysiological
478 recordings, we showed that activity in most V3-INs is correlated to fictive swimming
479 (Fig. 3) and is therefore appropriately timed to provide excitatory drive to MNs during
480 locomotion. Thus, this is the first direct evidence in any vertebrate preparation that V3-
481 INs are active during fictive locomotion, which provides supporting evidence that they
482 may participate in locomotor activity.
483
484 *V3-IN activity is necessary for motor neuron recruitment, but not necessary for rhythm*
485 *generation*
486 Given that V3-INs have been shown to affect the regularity and coordination of
487 locomotor activity in mice (Zhang et al., 2008), it was surprising that laser ablation of

488 V3-INs in larval zebrafish had no effect on episode duration, mean burst frequency, or
489 burst duration during fictive swimming in larval zebrafish (Table 1). One interpretation
490 of these findings is that despite similarities in gene expression and neurotransmitter
491 profile, premotor interneuron function is divergent between axial and tetrapod
492 locomotion. The latter argument has been advanced regarding the V2a-INs (Dougherty
493 and Kiehn, 2010; Dougherty et al., 2013); the different effects (or lack thereof) of V3-IN
494 ablation in zebrafish and mice may be a second example of the trend. An important
495 difference between the current study and mouse knock-out experiments is the mechanism
496 of ablation. In the current study, V3-INs were ablated acutely, and little time (~24 hours)
497 was given for circuit compensation. In the mouse experiments, on the other hand, V3-INs
498 were ablated or silenced chronically (Zhang et al., 2008; Rabe Bernhardt et al., 2012),
499 leaving opportunity for physiological compensation. Acute silencing experiments using
500 optogenetics could be performed in both species (Arrenberg et al., 2009; Hägglund et al.,
501 2013), and may demonstrate that this difference between species is due to the
502 experimental manipulation rather than the underlying neural circuit.

503 Finally, a subset of identified V2a excitatory spinal interneurons has been shown
504 to control the speed of locomotion in a variety of vertebrates (Zhong et al., 2011;
505 Ausborn et al., 2012; Ampatzis et al., 2014; Gosgnach et al., 2017). Of particular interest,
506 a recent study also ascribed a role for regulating locomotor amplitude/vigor to a
507 morphologically and functionally distinct subset of the V2a-INs (type II, non-bursting) in
508 larval and adult zebrafish (Song et al., 2018; Menelaou and McLean, 2019). Taken
509 together, these results indicate that the general population of V2a-INs is involved in
510 regulating both locomotor speed and amplitude. To date, however, a population of spinal

511 interneurons that selectively regulates locomotor amplitude has not been identified. Our
512 work provides evidence that, in zebrafish larvae, V3-INs contribute selectively to
513 locomotor amplitude. Specifically, we show that targeted ablation of V3-INs (Fig. 4)
514 reduces the proportion of active motor neurons during fictive swimming (Fig. 6E-F) but
515 does not affect the range of locomotor frequencies produced (Fig. 6C-D). Thus, we
516 propose that V3-INs are a source of excitation in the vertebrate locomotor neural circuitry
517 that regulates the amplitude of locomotor output independently of locomotor frequency.
518

519 *Conclusion*

520 The work presented here addressed an important concept regarding motor control;
521 specifically, a limited understanding of the cellular properties that produce locomotor
522 amplitude in vertebrates. We showed, directly for the first time, that V3-INs in zebrafish
523 larvae are active during *in vivo* fictive locomotion (Fig. 3) and contribute to motor neuron
524 recruitment. Importantly, targeted ablation of the V3-IN spinal cord population does not
525 affect locomotor frequency (speed; Fig. 6C-D), which clarifies their role in motor control
526 (amplitude) rather than rhythm generation (frequency). Thus, we propose that the V3-IN
527 population regulates locomotor amplitude independently of frequency, which is an
528 important functional difference between the V3-INs and the general population of V2a-
529 INs since the latter regulate both frequency and amplitude (Zhong et al., 2011; Ausborn
530 et al., 2012; Ampatzis et al., 2014; Gosgnach et al., 2017; Song et al., 2018; Menelaou
531 and McLean, 2019).

532 **REFERENCES**

533 Ampatzis K, Song J, Ausborn J, El Manira A (2014) Separate microcircuit modules of
534 distinct v2a interneurons and motoneurons control the speed of locomotion. Neuron
535 83:934–943 Available at:
536 http://linkinghub.elsevier.com/retrieve/pii/S0896627314006291 [Accessed October
537 19, 2017].

538 Arrenberg AB, Del Bene F, Baier H (2009) Optical control of zebrafish behavior with
539 halorhodopsin. Proc Natl Acad Sci U S A 106:17968–17973 Available at:
540 http://www.pnas.org/cgi/doi/10.1073/pnas.0906252106 [Accessed October 23,
541 2017].

542 Ausborn J, Mahmood R, El Manira A (2012) Decoding the rules of recruitment of
543 excitatory interneurons in the adult zebrafish locomotor network. Proc Natl Acad Sci
544 U S A 109:E3631-9 Available at:
545 http://www.pnas.org/cgi/doi/10.1073/pnas.1216256110 [Accessed October 19,
546 2017].

547 Bainbridge R (1958) The Speed of Swimming of Fish as Related to Size and to the
548 Frequency and Amplitude of the Tail Beat. J Exp Biol 35.

549 Balciunas D, Davidson AE, Sivasubbu S, Hermanson SB, Welle Z, Ekker SC (2004)
550 Enhancer trapping in zebrafish using the Sleeping Beauty transposon. BMC
551 Genomics 5.

552 Bellardita C, Kiehn O (2015) Phenotypic Characterization of Speed-Associated Gait
553 Changes in Mice Reveals Modular Organization of Locomotor Networks. Curr Biol
554 25:1426–1436 Available at: http://www.ncbi.nlm.nih.gov/pubmed/25959968

555 [Accessed October 23, 2017].
556 Bernhardt RR, Patel CK, Wilson SW, Kuwada JY (1992) Axonal trajectories and
557 distribution of GABAergic spinal neurons in wildtype and mutant zebrafish lacking
558 floor plate cells. J Comp Neurol 326:263–272.
559 Bertuzzi M, Ampatzis K (2018) Spinal cholinergic interneurons differentially control
560 motoneuron excitability and alter the locomotor network operational range. Sci Rep
561 8.
562 Borowska J, Jones CT, Zhang H, Blacklaws J, Goulding M, Zhang Y (2013) Functional
563 subpopulations of V3 interneurons in the mature mouse spinal cord. J Neurosci
564 33:18553–18565 Available at:
565 http://www.jneurosci.org/cgi/doi/10.1523/JNEUROSCI.2005-13.2013 [Accessed
566 October 23, 2017].
567 Briscoe J, Pierani A, Jessell TM, Ericson J (2000) A homeodomain protein code specifies
568 progenitor cell identity and neuronal fate in the ventral neural tube. Cell 101:435–
569 445 Available at: http://www.ncbi.nlm.nih.gov/pubmed/10830170 [Accessed
570 October 22, 2017].
571 Brustein E, Chong M, Holmqvist B, Drapeau P (2003) Serotonin Patterns Locomotor
572 Network Activity in the Developing Zebrafish by Modulating Quiescent Periods. J
573 Neurobiol.
574 Canales A, Park S, Kilias A, Anikeeva P (2018) Multifunctional Fibers as Tools for
575 Neuroscience and Neuroengineering. Acc Chem Res 51.
576 Chopek JW, Nascimento F, Beato M, Brownstone RM, Zhang Y (2018) Sub-populations
577 of Spinal V3 Interneurons Form Focal Modules of Layered Pre-motor Microcircuits.

578 Cell Rep 25.
579 Cole LK, Ross LS (2001) Apoptosis in the developing zebrafish embryo. Dev Biol
580 240:123–142.
581 Cope T, Pinter M (1995) The Size Principle: Still Working After All These Years.
582 Physiology 10:280–286.
583 Crone SA, Zhong G, Harris-Warrick R, Sharma K (2009) In mice lacking V2a
584 interneurons, gait depends on speed of locomotion. J Neurosci 29:7098–7109
585 Available at: http://www.jneurosci.org/cgi/doi/10.1523/JNEUROSCI.1206-09.2009
586 [Accessed October 23, 2017].
587 Dale N, Roberts A, Ottersen OP, Storm-Mathisen J (1987) The morphology and
588 distribution of "Kolmer-Agduhr cells", a class of cerebrospinal-fluid-contacting
589 neurons revealed in the frog embryo spinal cord by GABA immunocytochemistry.
590 Proc R Soc Lond B Biol Sci.
591 Danner SM, Zhang H, Shevtsova NA, Borowska-Fielding J, Deska-Gauthier D, Rybak
592 IA, Zhang Y (2019) Spinal V3 Interneurons and Left–Right Coordination in
593 Mammalian Locomotion. Front Cell Neurosci.
594 Deska-Gauthier D, Borowska-Fielding J, Jones CT, Zhang Y (2020) The temporal
595 neurogenesis patterning of spinal p3–V3 interneurons into divergent subpopulation
596 assemblies. J Neurosci 40.
597 Donley JM, Dickson KA (2000) Swimming kinematics of juvenile kawakawa tuna
598 (Euthynnus affinis) and chub mackerel (Scomber japonicus). J Exp Biol 203:3103–
599 3116 Available at: http://www.ncbi.nlm.nih.gov/pubmed/11003821 [Accessed
600 October 23, 2017].

601 Dougherty KJ, Kiehn O (2010) Firing and Cellular Properties of V2a Interneurons in the
602 Rodent Spinal Cord. J Neurosci 30:24–37 Available at:
603 http://www.jneurosci.org/cgi/doi/10.1523/JNEUROSCI.4821-09.2010.
604 Dougherty KJ, Zagoraiou L, Satoh D, Rozani I, Doobar S, Arber S, Jessell TM, Kiehn O
605 (2013) Locomotor Rhythm Generation Linked to the Output of Spinal Shox2
606 Excitatory Interneurons. Neuron 80:920–933.
607 Eklöf-Ljunggren E, Haupt S, Ausborn J, Dehnisch I, Uhlén P, Higashijima S, El Manira
608 A (2012) Origin of excitation underlying locomotion in the spinal circuit of
609 zebrafish. Proc Natl Acad Sci U S A 109:5511–5516 Available at:
610 http://www.pnas.org/cgi/doi/10.1073/pnas.1115377109 [Accessed October 19,
611 2017].
612 Ericson J, Rashbass P, Schedl A, Brenner-Morton S, Kawakami A, van Heyningen V,
613 Jessell TM, Briscoe J (1997) Pax6 controls progenitor cell identity and neuronal fate
614 in response to graded Shh signaling. Cell 90:169–180 Available at:
615 http://www.ncbi.nlm.nih.gov/pubmed/9230312 [Accessed October 22, 2017].
616 Gabriel JP, Ausborn J, Ampatzis K, Mahmood R, Eklöf-Ljunggren E, El Manira A
617 (2011) Principles governing recruitment of motoneurons during swimming in
618 zebrafish. Nat Neurosci 14:93–99 Available at:
619 http://www.nature.com/doifinder/10.1038/nn.2704 [Accessed October 19, 2017].
620 Gosgnach S, Bikoff JB, Dougherty KJ, El Manira A, Lanuza GM, Zhang Y (2017)
621 Delineating the diversity of spinal interneurons in locomotor circuits. J Neurosci 37.
622 Grillner S (2003) The motor infrastructure: From ion channels to neuronal networks. Nat
623 Rev Neurosci 4.

624 Grillner S, El Manira A (2020) Current principles of motor control, with special reference
625 to vertebrate locomotion. Physiol Rev 100.
626 Grillner S, Jessell TM (2009) Measured motion: searching for simplicity in spinal
627 locomotor networks. Curr Opin Neurobiol 19:572–586 Available at:
628 http://www.ncbi.nlm.nih.gov/pubmed/19896834 [Accessed October 20, 2017].
629 Gustafsson B, Pinter MJ (1984a) An investigation of threshold properties among cat
630 spinal alpha-motoneurones. J Physiol 357:453–483.
631 Gustafsson B, Pinter MJ (1984b) Relations among passive electrical properties of lumbar
632 alpha-motoneurones of the cat. J Physiol 356:401–431.
633 Hägglund M, Dougherty KJ, Borgius L, Itohara S, Iwasato T, Kiehn O (2013)
634 Optogenetic dissection reveals multiple rhythmogenic modules underlying
635 locomotion. Proc Natl Acad Sci U S A 110:11589–11594.
636 Heglund NC, Taylor CR, Mcmahon TA (1974) Scaling stride frequency and gait to
637 animal size: Mice to horses. Science (80- ) 186.
638 Henneman E, Somjen G, Carpenter DO (1965) Functional Significance of Cell Size in
639 Spinal Motoneurons. J Neurophysiol 28:560–580.
640 Higashijima S, Masino MA, Mandel G, Fetcho JR (2004) Engrailed-1 expression marks a
641 primitive class of inhibitory spinal interneuron. J Neurosci 24:5827–5839 Available
642 at: http://www.ncbi.nlm.nih.gov/pubmed/15215305 [Accessed October 19, 2017].
643 Hunter JR, Zweifel JR (1971) Swimming speed, tail beat frequency, tail beat amplitude,
644 and size in jack makerel, Trachurus symmetricus, and other fishes. Fish Bull
645 69:253–267 Available at: http://swfsc.noaa.gov/publications/CR/1971/7114.PDF
646 [Accessed October 23, 2017].

647 Jayne BC, Lauder GV (1995) Speed effects on midline kinematics during steady
648 undulatory swimming of largemouth bass, Micropterus salmoides. J Exp Biol
649 198:585–602 Available at: http://www.ncbi.nlm.nih.gov/pubmed/9318295
650 [Accessed October 23, 2017].
651 Kiehn O (2011) Development and functional organization of spinal locomotor circuits.
652 Curr Opin Neurobiol 21:100–109 Available at:
653 http://www.ncbi.nlm.nih.gov/pubmed/20889331 [Accessed October 20, 2017].
654 Kimura Y, Satou C, Fujioka S, Shoji W, Umeda K, Ishizuka T, Yawo H, Higashijima S
655 (2013) Hindbrain V2a Neurons in the Excitation of Spinal Locomotor Circuits
656 during Zebrafish Swimming. Curr Biol 23:843–849 Available at:
657 http://www.ncbi.nlm.nih.gov/pubmed/23623549 [Accessed October 20, 2017].
658 Kirby BB, Takada N, Latimer AJ, Shin J, Carney TJ, Kelsh RN, Appel B (2006) In vivo
659 time-lapse imaging shows dynamic oligodendrocyte progenitor behavior during
660 zebrafish development. Nat Neurosci.
661 Lin S, Li Y, Lucas-Osma AM, Hari K, Stephens MJ, Singla R, Heckman CJ, Zhang Y,
662 Fouad K, Fenrich KK, Bennett DJ (2019) Locomotor-related V3 interneurons
663 initiate and coordinate muscles spasms after spinal cord injury. J Neurophysiol.
664 Ljunggren EE, Haupt S, Ausborn J, Ampatzis K, El Manira A (2014) Optogenetic
665 activation of excitatory premotor interneurons is sufficient to generate coordinated
666 locomotor activity in larval zebrafish. J Neurosci 34:134–139 Available at:
667 http://www.jneurosci.org/cgi/doi/10.1523/JNEUROSCI.4087-13.2014 [Accessed
668 October 19, 2017].
669 McLean DL, Fan J, Higashijima S, Hale ME, Fetcho JR (2007) A topographic map of

670 recruitment in spinal cord. Nature 446:71–75 Available at:
671 http://www.ncbi.nlm.nih.gov/pubmed/17330042 [Accessed October 19, 2017].
672 McLean DL, Fetcho JR (2004) Ontogeny and innervation patterns of dopaminergic,
673 noradrenergic, and serotonergic neurons in larval zebrafish. J Comp Neurol 480:38–
674 56 Available at: http://www.ncbi.nlm.nih.gov/pubmed/15515022 [Accessed October
675 19, 2017].
676 Mendell LM (2005) The size principle: A rule describing the recruitment of
677 motoneurons. J Neurophysiol 93:3024–3026.
678 Menelaou E, McLean DL (2019) Hierarchical control of locomotion by distinct types of
679 spinal V2a interneurons in zebrafish. Nat Commun 10.
680 Menelaou E, VanDunk C, McLean DL (2014) Differences in the morphology of spinal
681 V2a neurons reflect their recruitment order during swimming in larval zebrafish. J
682 Comp Neurol 522:1232–1248 Available at: http://doi.wiley.com/10.1002/cne.23465
683 [Accessed October 19, 2017].
684 Miyasaka N, Morimoto K, Tsubokawa T, Higashijima S, Okamoto H, Yoshihara Y
685 (2009) From the olfactory bulb to higher brain centers: genetic visualization of
686 secondary olfactory pathways in zebrafish. J Neurosci 29:4756–4767 Available at:
687 http://www.jneurosci.org/cgi/doi/10.1523/JNEUROSCI.0118-09.2009 [Accessed
688 October 20, 2017].
689 Montgomery JE, Wahlstrom-Helgren S, Wiggin TD, Corwin BM, Lillesaar C, Masino
690 MA (2018) Intraspinal serotonergic signaling suppresses locomotor activity in larval
691 zebrafish. Dev Neurobiol.
692 Montgomery JE, Wiggin TD, Rivera-Perez LM, Lillesaar C, Masino MA (2016)

693 Intraspinal serotonergic neurons consist of two, temporally distinct populations in
694 developing zebrafish. Dev Neurobiol 76:673–687 Available at:
695 http://doi.wiley.com/10.1002/dneu.22352 [Accessed October 19, 2017].
696 Montgomery KL, Yeh AJ, Ho JS, Tsao V, Iyer SM, Grosenick L, Ferenczi EA, Tanabe
697 Y, Deisseroth K, Delp SL, Poon ASY (2015) Wirelessly powered, fully internal
698 optogenetics for brain, spinal and peripheral circuits in mice. Nat Methods 12.
699 Müller UK, van Leeuwen JL (2004) Swimming of larval zebrafish: ontogeny of body
700 waves and implications for locomotory development. J Exp Biol 207:853–868
701 Available at: http://www.ncbi.nlm.nih.gov/pubmed/14747416 [Accessed October
702 22, 2017].
703 Muto A, Lal P, Ailani D, Abe G, Itoh M, Kawakami K (2017) Activation of the
704 hypothalamic feeding centre upon visual prey detection. Nat Commun.
705 Pierani A, Brenner-Morton S, Chiang C, Jessell TM (1999) A sonic hedgehog-
706 independent, retinoid-activated pathway of neurogenesis in the ventral spinal cord.
707 Cell 97:903–915 Available at: http://www.ncbi.nlm.nih.gov/pubmed/10399918
708 [Accessed October 22, 2017].
709 Preibisch S, Saalfeld S, Tomancak P (2009) Globally optimal stitching of tiled 3D
710 microscopic image acquisitions. Bioinformatics.
711 Rabe Bernhardt N, Memic F, Gezelius H, Thiebes A-L, Vallstedt A, Kullander K (2012)
712 DCC mediated axon guidance of spinal interneurons is essential for normal
713 locomotor central pattern generator function. Dev Biol 366:279–289 Available at:
714 http://linkinghub.elsevier.com/retrieve/pii/S0012160612001807 [Accessed October
715 20, 2017].

716 Samineni VK et al. (2017) Fully implantable, battery-free wireless optoelectronic devices
717 for spinal optogenetics. Pain 158.
718 Satou C, Kimura Y, Hirata H, Suster ML, Kawakami K, Higashijima S -i. (2013)
719 Transgenic tools to characterize neuronal properties of discrete populations of
720 zebrafish neurons. Development 140:3927–3931 Available at:
721 http://www.ncbi.nlm.nih.gov/pubmed/23946442 [Accessed October 20, 2017].
722 Schäfer M, Kinzel D, Winkler C (2007) Discontinuous organization and specification of
723 the lateral floor plate in zebrafish. Dev Biol 301:117–129 Available at:
724 http://linkinghub.elsevier.com/retrieve/pii/S001216060601219X [Accessed October
725 25, 2017].
726 Schindelin J, Arg I, Arganda-Carreras I, a-Carreras, Frise E, Kaynig V, Longair M,
727 Pietzsch T, Preibisch S, Rueden C, Saalfeld S, Schmid B, Tinevez J-Y, White D,
728 Hartenstein V, Eliceiri K, Tomancak P, Cardona A (2012) Fiji: an open-source
729 platform for biological-image analysis. Nat Methods 9.
730 Song J, Dahlberg E, El Manira A (2018) V2a interneuron diversity tailors spinal circuit
731 organization to control the vigor of locomotor movements. Nat Commun.
732 Tytell ED (2004) The hydrodynamics of eel swimming II. Effect of swimming speed. J
733 Exp Biol 207:3265–3279 Available at:
734 http://www.ncbi.nlm.nih.gov/pubmed/15326203 [Accessed October 23, 2017].
735 Van Raamsdonk W, Bosch TJ, Smit-Onel MJ, Maslam S (1996) Organisation of the
736 zebrafish spinal cord: distribution of motoneuron dendrites and 5-HT containing
737 cells. Eur J Morphol.
738 Videler JJ, Müller UK, Stamhuis EJ (1999) Aquatic vertebrate locomotion: Wakes from

739 body waves. J Exp Biol 202.
740 Wardle, Videler, Altringham (1995) Tuning in to fish swimming waves: body form,
741 swimming mode and muscle function. J Exp Biol 198.
742 Webb PW (1975) Hydrodynamics and energetics of fish propulsion. Bull Fish Res Board
743 Canada 190:1–159 Available at: http://www.dfo-mpo.gc.ca/library/1486.pdf
744 [Accessed October 23, 2017].
745 Webb PW, Kostecki PT, Stevens ED (1984) The Effect of Size and Swimming Speed on
746 Locomotor Kinematics of Rainbow Trout. J Exp Biol 109.
747 Wiggin TD, Anderson TM, Eian J, Peck JH, Masino MA (2012) Episodic swimming in
748 the larval zebrafish is generated by a spatially distributed spinal network with
749 modular functional organization. J Neurophysiol 108:925–934 Available at:
750 http://jn.physiology.org/cgi/doi/10.1152/jn.00233.2012 [Accessed October 19,
751 2017].
752 Yang L, Rastegar S, Strähle U (2010) Regulatory interactions specifying Kolmer-Agduhr
753 interneurons. Development 137:2713–2722 Available at:
754 http://dev.biologists.org/cgi/doi/10.1242/dev.048470 [Accessed October 20, 2017].
755 Zajac FE, Faden JS (1985) Relationship among recruitment order, axonal conduction
756 velocity, and muscle-unit properties of type-identified motor units in cat plantaris
757 muscle. J Neurophysiol 53:1303–1322.
758 Zhang Y, Narayan S, Geiman E, Lanuza GM, Velasquez T, Shanks B, Akay T, Dyck J,
759 Pearson K, Gosgnach S, Fan CM, Goulding M (2008) V3 Spinal Neurons Establish
760 a Robust and Balanced Locomotor Rhythm during Walking. Neuron 60:84–96
761 Available at: http://linkinghub.elsevier.com/retrieve/pii/S0896627308008064

762 [Accessed October 20, 2017].

763 Zhong G, Sharma K, Harris-Warrick RM (2011) Frequency-dependent recruitment of

764 V2a interneurons during fictive locomotion in the mouse spinal cord. Nat Commun

765 2:274 Available at: http://www.nature.com/doifinder/10.1038/ncomms1276

766 [Accessed October 19, 2017].

767 **LEGENDS**

768 **Figure 1. V3-INs are identified by co-localization of *vglut2a:DsRed* and**
769 ***nkx2.2a:mEGFP* transgene expression in neurons located in the ventromedial spinal**
770 **cord.** (A) Whole-mount *Tg(nkx2.2a:mEGFP)*$^{vu17}$;*Tg(vglut2a:DsRed)*$^{nns9}$ double
771 transgenic zebrafish larva. (B-D) A representative single confocal optical section of the
772 spinal cord exhibiting: (B) *nkx2.2a:mEGFP* expression, (C) *vglut2a:DsRed* expression,
773 and (D) overlayed *nkx2.2a:mEGFP* and *vglut2a:DsRed* expression. The boundaries of the
774 spinal cord and central canal are illustrated by solid and dashed white lines, respectively,
775 in panel B. White triangles indicate neurons that co-express both transgenes and the black
776 triangle indicates the only *vglut2a:DsRed* neuron ventral to the central canal that did not
777 co-express *nkx2.2a:mEGFP* in the field of view. Scale bars: 1 mm in A and 10 µm in B-
778 D.

779

780 **Figure 2. Distribution of V3-IN Cell Bodies in the Spinal Cord.** (A) Maximum
781 intensity projection of a confocal stack of the spinal cord of a 5 dpf
782 Tg(*vglut2a:DsRed*)$^{nns9}$ zebrafish larva. The dashed white outline indicates the region of
783 the cord in which cells were quantified. The solid white outline is the region of the image
784 shown at higher magnification in (B). (B) A higher magnification field of view. White
785 circles indicate V3 neurons, black triangles indicate DRG neurons located lateral of the
786 spinal cord. (C) Distribution of location of all quantified V3-INs (red dots) projected in
787 the coronal plane of the spinal cord. The schematic outline of the spinal cord (solid grey
788 line), as well as the location of the central canal (cc) and Mauthner axon (m), are
789 approximate. The heavy black line indicates the line of best fit that best describes the axis

790 of the V3-IN population. (D-G) The windowed moving average of V3-IN density along
791 the rostrocaudal axis (D; window width: 250 µm), mediolateral axis (E; window width:
792 15% SC radius), dorsoventral axis (F; window width: 15% SC radius), and along the
793 population axis illustrated in panel C (G; window width: 15% SC radius). Black lines are
794 the mean, grey area indicates the standard deviation. SC: spinal cord. Scale bar: 100 µm
795 in A and 19 µm in B.
796
797 **Figure 3. V3-IN activity is temporally correlated to fictive locomotion.** (A) Schematic
798 representing the number and distribution of V3-INs (green circles) along the rostrocaudal
799 axis of the spinal cord monitored during calcium imaging experiments. (B) Each V3-IN
800 in the field of view in Tg(*vglut2a:Gal4ff*)$^{nns20}$;Tg(*UAS:GCaMP6s*)$^{nk13a}$ double transgenic
801 larvae was assigned a ROI during spontaneous fictive swimming. Panels in (A) show raw
802 GCaMP6s fluorescence (F) and correspond to numbered time-points in (B). Bottom panel
803 in A shows calculated ΔF/F between 3 and 7 s time-points. Dashed lines represent ventral
804 boundary of the spinal cord. (B) Synchronized recordings of GCaMP6s fluorescence
805 (top) and fictive swimming (bottom) allowed identification of swimming-related
806 neuronal activity.
807
808 **Figure 4. Targeted ablation of V3-INs is both efficient and spatially restricted.** (A-B)
809 Confocal stacks of the same Tg(*vglut2a:DsRed*)$^{nns9}$ zebrafish larva before (A) and 12
810 hours after (B) laser ablation of the V3-INs in the region indicated (red dashed lines). (C-
811 D) A magnified view of two V3-INs before (left) and after (right) a single cell laser
812 ablation. Scale bars: 20 µm in A and B and 5 µm in C and D.

813

814 **Figure 5. Spinal neurons loaded with rhodamine-2 AM dye are definitively**

815 **identified as MNs.** (A) The EGFP-expressing *parga*$^{mn2Et}$ enhancer trap line (A, green)

816 was labeled with antibodies to choline acetyl transferase (ChAT; A′, red). Colabeling

817 (A″) of EGFP with ChAT antibodies indicated that EGFP expression in the *parga*$^{mn2Et}$

818 line is a marker of spinal motor neurons. White arrowheads indicate ChAT-positive cells

819 that do not contain EGFP (non-MNs). (B) Live *parga*$^{mn2Et}$ larvae were anesthetized,

820 skinned, and incubated in rhodamine-2 AM dye (Rhod-2, AM). EGFP expression (B,

821 green) and Rhod-2, AM labeling (B′, red), showed that Rhod-2, AM specifically labeled

822 all motor neurons (B″). White arrowheads indicate two Rhod-2, AM-labeled cells that did

823 not contain EGFP. Scale bar: 20 μm.

824

825 **Figure 6. V3-IN laser ablation reduces the proportion of motor neurons that are**

826 **active during fictive swimming.** MNs in *Tg(vglut2a:DsRed)*$^{nns9}$ larvae were loaded with

827 Calcium Green-1 AM dye and assigned ROIs during recording. Synchronous MN

828 fluorescence and fictive swimming recordings were compared between Control, V3-IN

829 Ablated, and Sham ablated preparations. (A and B) Pseudocolor Calcium Green-1 AM

830 fluorescence panels correspond to numbered time-points in aligned ΔF/F (each gray line

831 represents a MN) and peripheral nerve traces in a Control preparation (A) and a V3-IN

832 Ablated preparation (B). Color indicates fluorescence intensity. (C-F) Cumulative

833 probability distributions and mean Peak Burst Frequencies (C and D) and percent of MNs

834 active (10% ΔF/F threshold) during fictive swimming episodes (E and F). Asterisks

835 represent significant differences. Error bars represent SD.

836

837 **Table 1. Measures of the episodic and burst properties from peripheral nerve**

838 **recordings during fictive locomotion in zebrafish larvae.** All values presented as

839 mean, standard deviation.

840 **Figure 1**

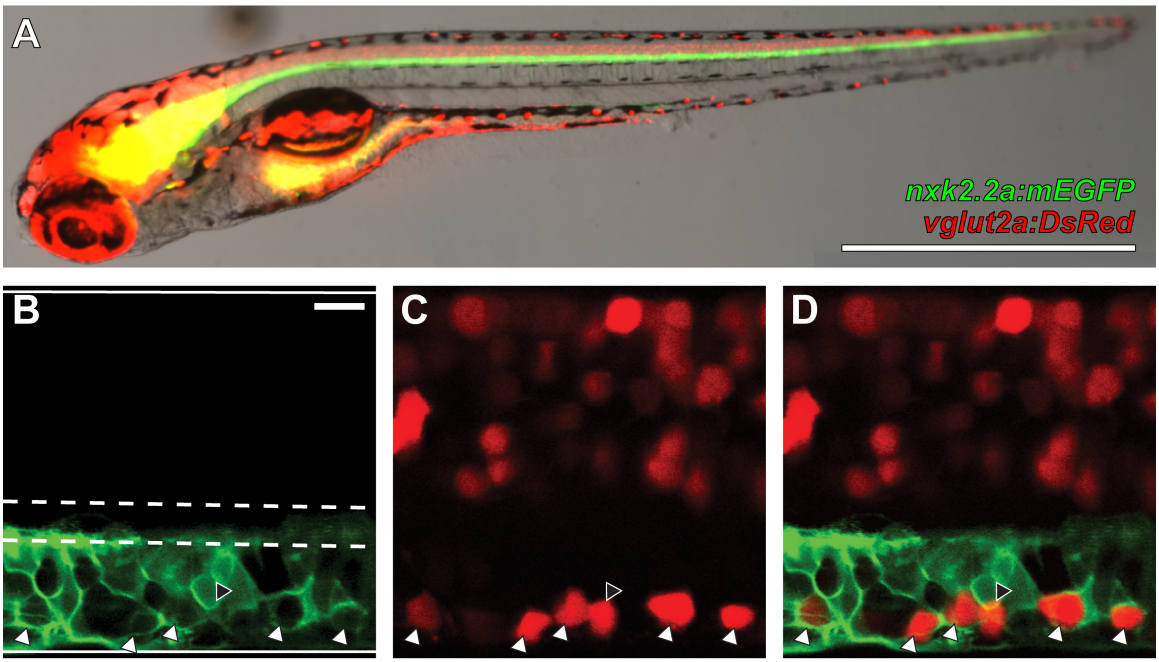


841

842 **Figure 2**

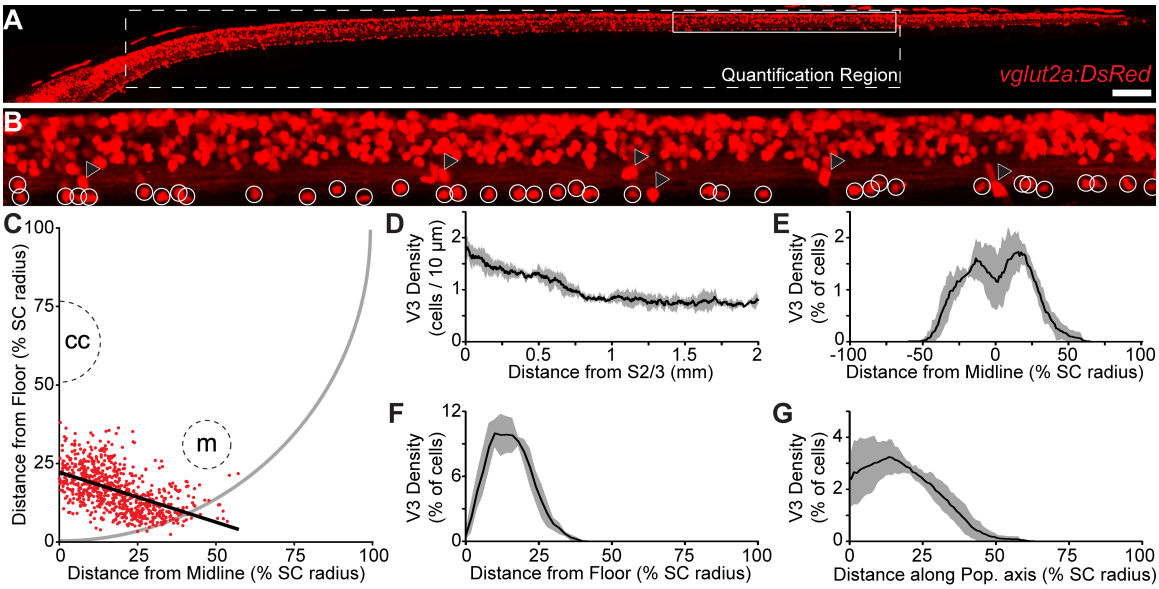


843

844 **Figure 3**

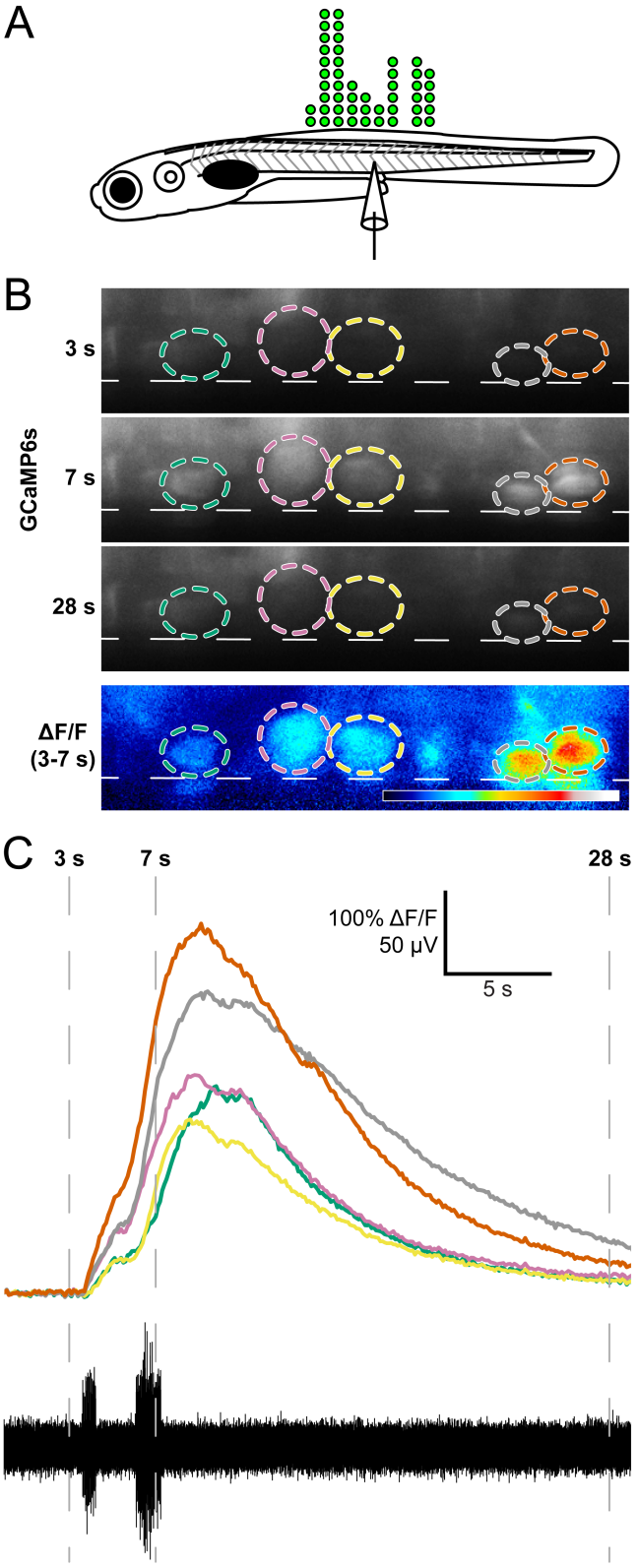


845

846 **Figure 4**

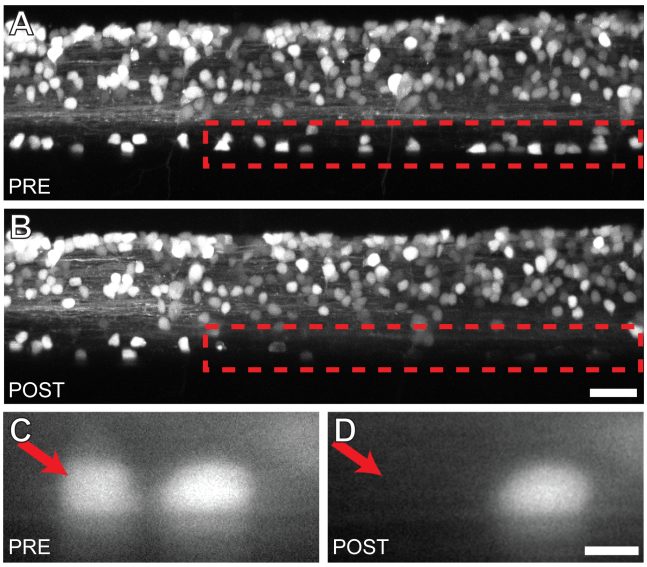


847

848 **Figure 5**

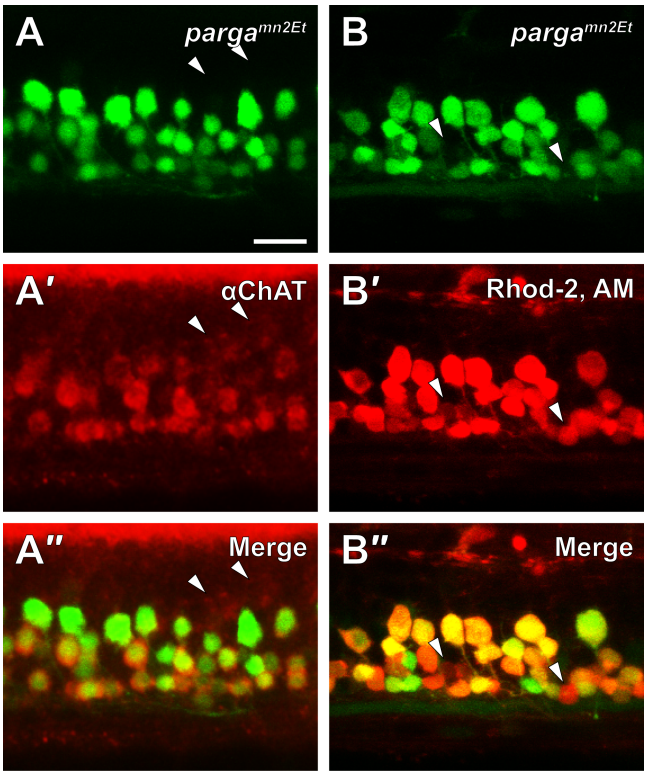


849

850 **Figure 6**

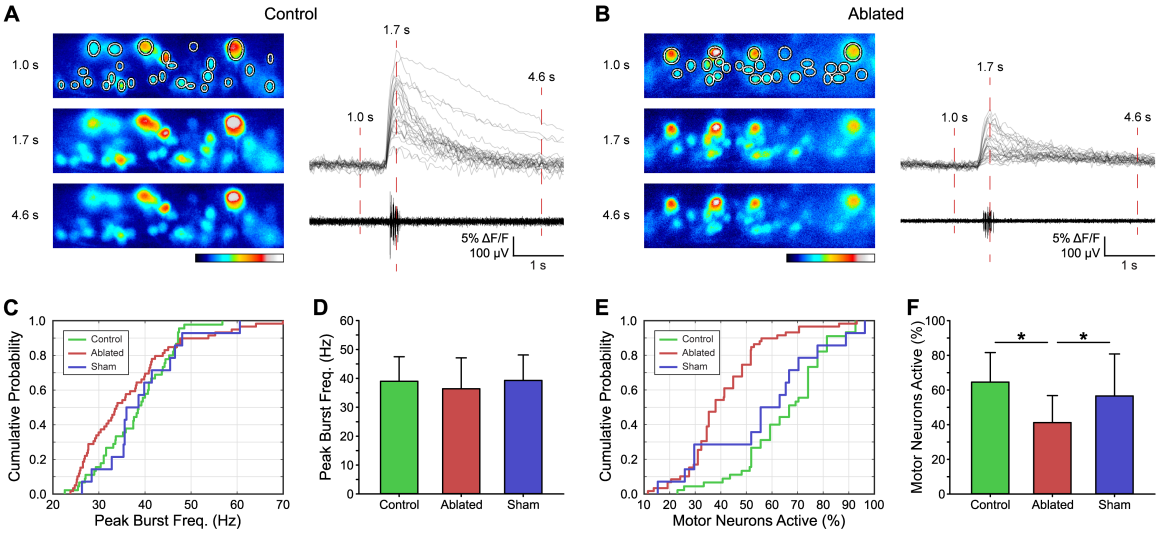


851

852 **Table 1**

| | | Episode Duration (ms) | Peak Burst Frequency (Hz) | Burst Duration (ms) |
|---|---|---|---|---|
| **Control** (n = 6 larvae) | | 720, SD713 | 25.7, SD3.4 | 10.4, SD2.8 |
| **Ablated** (n = 6 larvae) | | 524, SD223 | 28.3, SD1.9 | 11.8, SD2.2 |
| **Sham** (n = 6 larvae) | | 878, SD642 | 28.2, SD3.8 | 11.4, SD2.7 |
| **ANOVA** | **F** | 0.58 | 1.30 | 0.42 |
| | **p** | 0.57 | 0.30 | 0.67 |

853